Mon. Not. R. Astron. Soc. **318**, 440–452 (2000)

Investigating the structure of the accretion disc in WZ Sge from multiwaveband time-resolved spectroscopic observations – II

Elena Mason,[1,2]★ Warren Skidmore,[1,3] Steve B. Howell,[1,2] David R. Ciardi,[4] Stuart Littlefair[5] and V. S. Dhillon[5]

[1]*Department of Physics and Astronomy, University of Wyoming, PO Box 3905, University Station, Laramie, WY 82071, USA*
[2]*Astrophysics Group, Planetary Science Institute, 620 N. 6th Avenue, Tucson, AZ 85705, USA*
[3]*School of Physics and Astronomy, University of St Andrews, North Haugh, St Andrews, Fife KY16 9SS*
[4]*Department of Astronomy, 211 Bryant Space Science Center, PO Box 112055, University of Florida, Gainesville, FL 32611, USA*
[5]*Department of Physics and Astronomy, University of Sheffield, Sheffield S3 7RH*

Accepted 2000 June 9. Received 2000 June 9; in original form 1999 December 13

ABSTRACT

We present our second paper describing multiwaveband time-resolved spectroscopy of WZ Sge. We analyse the evolution of both optical and IR emission lines throughout the orbital period and find evidence, in the Balmer lines, for an optically thin accretion disc and an optically thick hotspot. Optical and IR emission lines are used to compute radial velocity curves. Fits to our radial velocity measurements give an internally inconsistent set of values for K_1, γ and the phase of red-to-blue crossing. We present a probable explanation for these discrepancies, and provide evidence for similar behaviour in other short orbital period dwarf novae. Selected optical and IR spectra are measured to determine the accretion disc radii. Values for the disc radii are found to be strongly dependent on the assumed WD mass and binary orbital inclination. However, the separation of the peaks in the optical emission line (i.e., an indication of the outer disc radius) has been found to be constant during all phases of the supercycle period over the last 40 years.

Key words: accretion, accretion discs – binaries: close – stars: individual: WZ Sge – novae, cataclysmic variables.

1 INTRODUCTION

Dwarf novae, among the cataclysmic variables (CVs), are semidetached binary star systems where a white dwarf (primary star) accretes gas from a cool companion (secondary star). The gas from the secondary star accretes through the inner Lagrangian point (L1) into the primary Roche lobe and slowly spirals in toward the white dwarf. The in-flowing gas forms an accretion disc which orbits around the white dwarf before actually being accreted on to the primary star. During the time the gas is within the accretion disc, current theory tells us that half of the gravitational energy of the gas is radiated outward, while that which remains heats the accretion disc. Indeed, most of the visible and IR light output by a typical dwarf novae is from the accretion disc (Warner 1995; Ciardi et al. 1998). Emission lines seen in the spectra of a dwarf nova arise from the vicinity of the accretion disc and can be double-peaked as a result of the Doppler motions of the disc within the binary (Horne & Marsh 1986). The velocity of the material within the disc, together with the emitted flux distribution over the disc, determines the line profile shape. Consequently, spectral line analysis is a fundamental method employed to understand the physical state of the accretion disc and its spatial flux distribution. The most common emission lines used in such analyses are those due to hydrogen and helium.

In this paper we continue the analysis of the accretion disc in WZ Sge that was started in Skidmore et al. (2000, hereafter Paper I). Paper I presented Doppler tomography of optical and IR disc emission lines, as well as ratioed Doppler maps. General conclusions reached there indicated different optical depths at the hotspot and the accretion disc, and an accretion disc structure dissimilar to those predicted by models. In this paper (Paper II) we perform spectral analysis by direct measurements of the emission-line profiles. We organize the present paper in three main sections. Section 2 describes the orbital phase dependence of Hα, Hβ and IR emission lines. Section 3 presents newly determined radial velocity curves using optical and IR emission lines. We show that the amplitude and phase zero of the radial velocity curves are systematically biased, and that this is because of different gas opacities in the hotspot and the accretion disc, the hotspot having a larger opacity than the accretion disc. We further develop the idea of increasing hotspot contamination in systems where the difference between the optical depth in the hotspot and the accretion

★ E-mail: elena@psi.edu

Table 1. Log of the observations of WZ Sge used in this analysis. Velocity dispersion is stated for the line used; it is not the mean velocity dispersion of the complete data set. († average value for all three lines.)

Date of observations	Wavelength range (Å)	Emission lines	Dispersion (Å pixel)	App. dispersion (km s^{-1})	Exposure time (s)	Run duration (h)	Orbits covered	Number of spectra
27/07/96	6375–6780	Hα	0.40	18.1	40	5.51	4.1	237
27/07/96	4590–4995	Hβ	0.40	24.6	40	5.03	3.7	239
28/07/96	6375–6780	Hα	0.40	18.1	40	4.07	3.0	139
28/07/96	4590–4995	Hβ	0.40	24.6	40	4.10	3.0	137
28/05/97	18000–24600	Brγ, Brδ, He I	13.2	193†	480	2.70	2.0	18
08/08/98	10300–13400	Paβ	6.22	145.6	240	6.73	3.5	30

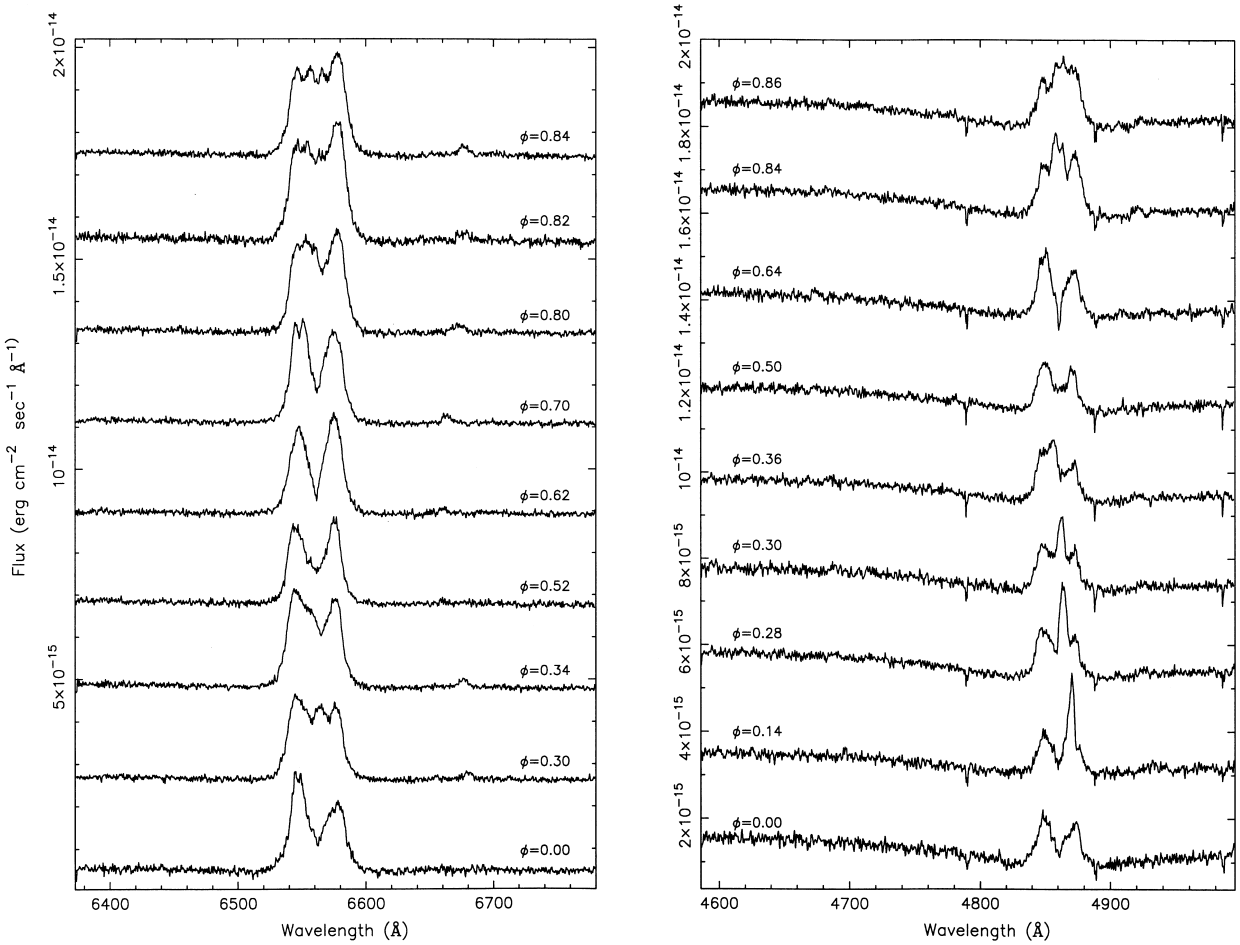

Figure 1. Sample Hα and Hβ phase-binned spectra (50 bins per orbit). Each spectrum is offset from the one below by 2.1×10^{-15} erg cm^{-2} s^{-1} Å^{-1}, and each bin is labelled with the mid-orbital bin phase based on the optical photometric eclipse ephemeris listed in Paper I. Note that the Hα spectra show a weak He I emission line (λ6678 Å), which follows the Hα S-wave motion (see trailed-spectrum in fig. 1 of Paper I). The narrow 'absorption features' seen in the Hβ spectra are due to bad pixels. *Note:* the left and right panels have the same flux units.

disc is large, these systems being short orbital period, low mass transfer rate dwarf novae. In Section 4 we present our determinations for the accretion disc radii and compare our values with previously reported determinations.

Complete details concerning the data set used here (see Table 1) are given in Paper I. All data are phased according to the photometric eclipse ephemeris stated in table 7 of Paper I. Optical spectra of WZ Sge were grouped into 50 phase bins per orbit in order to improve the signal-to-noise ratio of the data.

2 EMISSION LINES

We analyse the emission lines evolution by inspecting their profile, measuring the fluxes, and computing the Balmer decrement (last analysis on optical spectra only). Fig. 4 summarizes the results from each analysis.

2.1 The line profiles

Figs 1 and 2 present a sample of optical and IR spectra respectively to show the complex emission-line profiles and their dramatic evolution throughout an orbital period. Both optical and IR emission-line profiles evolve similarly and owe most of their changes to the variable strength of the hotspot around the orbit. Phases 0.3, 0.5, 0.84 and 0.63 are particularly suitable to point out the hotspot evolution over the orbit.

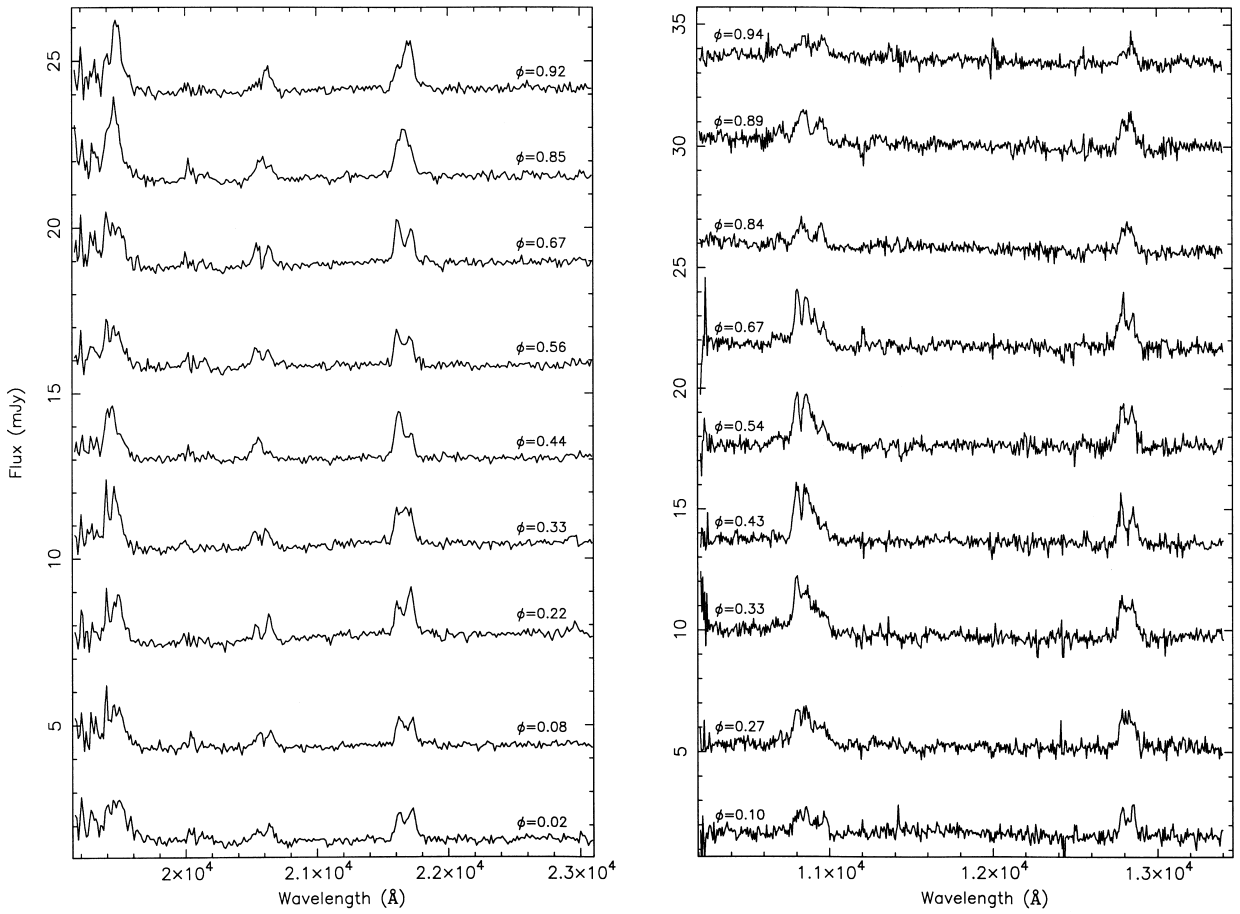

Figure 2. IR spectra in the *K* and **J** bands. Spectra are labelled with the phase at mid-exposure time as set by the photometric eclipse ephemeris listed in Paper I. Flux is in mJy and the offset between each spectra is 2.8 and 4.0 mJy for *K* and *J* spectra respectively. *Note:* the left and right panels have the same flux units.

Inspection shows that phase 0.3 is when the hotspot, in both Hα and Hβ emission lines, is at the centre of the accretion disc emission, i.e., has zero radial velocity with respect to an observer comoving with the white dwarf. From the system geometry determined in Paper I we expect the hotspot in the middle of the accretion disc emission line at phase $\sim$0.3 *only* if the gas at the stream–disc impact region has just the stream velocity (see Fig. 4). This condition implies that the accretion disc density is low enough such that the gas at the stream–disc impact region keeps its stream velocity with little effect from the Keplerian motion of the underlying accretion disc material. In the IR spectra the phase of the hotspot zero radial velocity occurs slightly later, i.e., at phase 0.33. Phase binning of the optical spectra with the same time resolution of the IR spectra has showed that such a delay is significant and implies different velocities of the hotspot gas in different wavebands. We explain such a phase delay with the hotspot emission from different lines spreading along the stream trajectory (Fig. 4).

The hotspot appears again at the centre of the emission line at phase 0.84, both in the optical and IR spectra. The expected phase for the optical spectra is 0.80 in the assumption of symmetric and isotropic hotspot emission. Further evidence for asymmetric and anisotropic hotspot emission is in the hotspot profile which appears double-peaked at phase 0.84. This feature is real, as it is common to both Hα and Hβ *binned* spectra and is visible for a phase interval of $\leq$0.5 (see also the trailed spectrograms in fig. 1 of Paper I). A detailed study of the double structure is beyond the scope of this paper. The lower spectral resolution in the *J* and *K* bands does not resolve such a feature if present (the hotspot peak separation is $\simeq$9 Å in the Balmer lines).

Phase $\sim$0.53 is when we expect the maximum hotspot blueshift and enhanced blue peak emission in the accretion disc lines. Observations do not confirm this expectation, and show redshifted and blueshifted peaks of roughly equal strength between phases 0.5 and 0.56, both in the optical and IR spectra. We explain this observation with little or no contribution from the hotspot to the overall emission-line flux. This is also evidence of the anisotropic hotspot emission.

Asymmetries in the accretion disc are evident in the Hα emission line, which displays a stronger red-shifted peak at phase 0.63. Doppler maps in Paper I show asymmetric accretion discs also in the Hβ, Brγ, He I, and Brδ lines. The accretion disc emission-line profile evolves from a shallow U-shaped profile to a V-shaped profile, between phase 0.5 and 0.63. This is particularly evident in the optical spectra; among IR observations, only the *J*-band spectra show similar evolution. Horne & Marsh (1986) predict U-shaped emission-line profiles for optically thin accretion discs, and V-shaped profiles for the optically thick case. This might suggest that the changing profile of the emission lines is evidence that some areas of the disc have optically thin line emission and some have optically thick line emission.

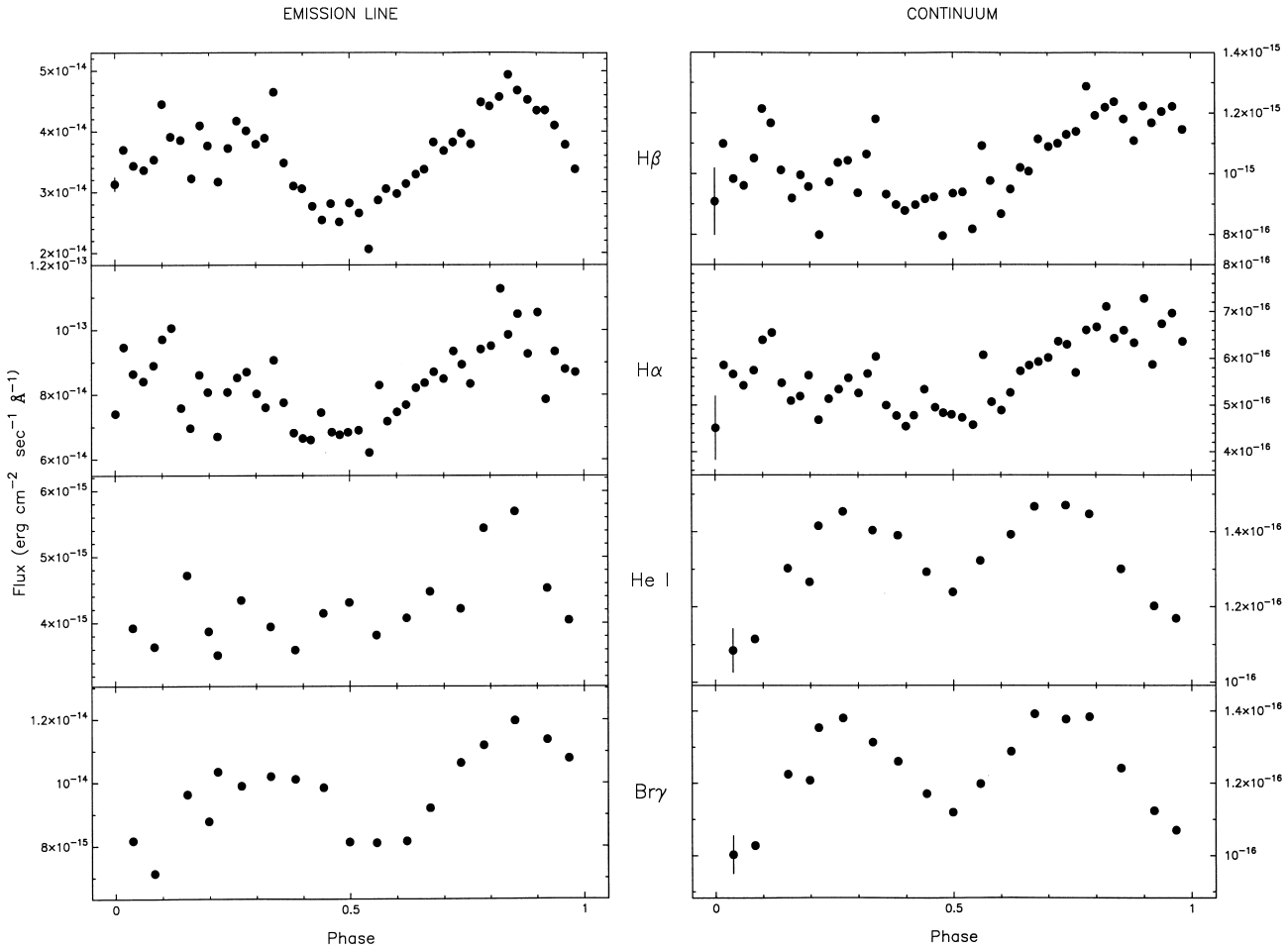

Figure 3. Left: the line flux for each emission line versus the orbital phase; Right: the continuum flux underlying the emission lines versus orbital phase. Fluxes measured at phases 0.3, 0.5 and 0.84 are in Table 2. Both emission-line and continuum fluxes were measured using the *e-e* command in IRAF task *splot*; fitting was not attempted. Average uncertainties on measurements are plotted on the first data point in each panel; errorbars on Hα, Brγ, and He I 2.06-μm emission lines are smaller than the data point size. *Note:* the left and right panels have the same flux units.

2.2 Line flux

The emission-line flux was measured by manually marking the position of line wings with the cursor and summing up the flux from each pixel in between; the continuum flux corresponding to a linear interpolation of the same two cursor position was automatically subtracted during the line flux measurements. Each of the emission lines measured (with the exception of the Paβ line) shows quite strong modulations apparently correlated with the line profile evolution (Fig. 3). The modulations display maxima at phases 0.84 and 0.3, and a minimum at phase 0.5. Thus the hotspot shows stronger emission when viewed from the outside (phase 0.84) and from the inside (0.3), while it does not contribute significantly to the emission-line flux when viewed from upstream (phase 0.5). Assuming that the flux at phase 0.5 is due only to the accretion disc (see Figs 1 and 2, and the previous subsection), we can compute the relative contribution by the hotspot to the total emission-line flux. At phase 0.84 the hotspot emits 50 per cent of the total line flux in Hβ, and $\sim$30 per cent in Hα and the IR lines. When viewed from the inside, the hotspot relative contribution decreases to 38 per cent in Hβ and to $\sim$20 per cent in Hα and Brγ. The He I 2.06 μm line does not display an evident hump at phase 0.3 and so the relative hotspot contribution was not computed there. Assuming a spherical hotspot with radius $S = 3.1 \times 10^8$ cm (Smak 1993), cylindrical accretion disc with thickness $2H \sim 3.8 \times 10^8$ cm,[1] and inclination $i = 75°$ (Smak 1993), the decrease of the hotspot flux from phase 0.84 to phase 0.30 due to occultation by an optically thick disc is 70 per cent. We observe a decrease of only 30 per cent in Hβ, and $\sim$50 per cent in Hα and Brγ. Thus, either the accretion disc gas is at least partially transparent to the hotspot emission-line flux, or the assumed geometry inappropriate.

The continuum light curve is expected to be double-humped as already observed by Ciardi et al. (1998) in the IR, and by Patterson et al. (1996) and Skidmore (1998) in the optical. The right-hand panel of Fig. 3 shows that only our *K*-band continuum measurements match with previous observations. The optical continuum shows large uncertainties on each data point and poor modulation throughout the orbit, as the method used to measure line and continuum flux does not take into account the underlying white dwarf absorption. The IR spectra, which do not show any evidence of white dwarf features, have the expected double-humped structure and smaller uncertainties in the continuum light curves. Fluxes from the Paβ emission line and its underlying

[1] The value was derived computing the scaleheight H as given in Williams & Shipman (1988), assuming a uniform temperature $T = 6000$ K in the accretion disc and a white dwarf mass of $M_{WD} = 0.82\,M_\odot$ (Paper I).

Table 2. The maximum and minimum fluxes, and the flux near phase 0.3, as measured in each emission line. Flux units are erg cm^2 s^{-1} Å^{-1}. The minimum fluxes are observed about phase 0.5 and are believed to correspond to the phase when there is no contribution from the hotspot. The maximum flux is observed at phase 0.84 when the hotspot is viewed from the outside. Phase 0.3 is the phase when the hotspot is viewed from the inside.

Line	Max Flux	Min Flux	Flux at $\phi \sim 0.3$
Hα	11.00×10^{-14}	6.75×10^{-14}	8.80×10^{-14}
Hβ	4.95×10^{-14}	2.65×10^{-14}	4.00×10^{-14}
Brγ	1.19×10^{-14}	1.01×10^{-14}	8.32×10^{-15}
He I 2.06 μm	5.67×10^{-15}	3.54×10^{-15}	–

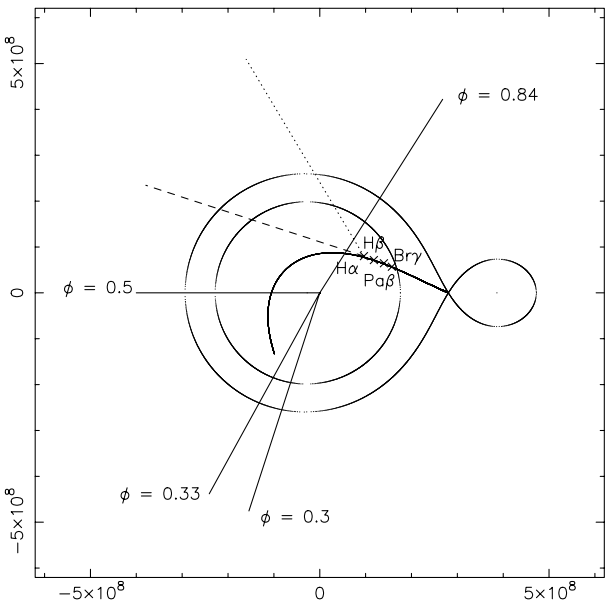

Figure 4. The Roche lobe geometry of WZ Sge corresponding to a white dwarf mass of 0.82 $M_\odot$ (Paper I), and the secondary star mass (0.058 $M_\odot$) computed by Smak (1993). Units on both the *x*- and *y*-axes are metres. Straight full lines mark the line of sight at the phases considered in the text. Dashed and dotted lines show the directions of stream and Keplerian velocity respectively for the illustrative case of Hα hotspot position. Crosses along the stream trajectory qualitatively mark the hotspot position for each emission line as predicted by our results. From left to right: Hα, Hβ, Paβ and Brγ in order of increasing excitation energy and gas temperature.

continuum have not been reported in Fig. 3 and Table 2, because the data show variations throughout the run of observation. The run covered about four cycles, and variations between cycles do not appear to be correlated. We cannot say whether this is due to intrinsic variability of the emitting source or to external causes.

2.3 The Balmer decrement

We measured the Balmer decrement for both the accretion disc and the hotspot region to check for different opacities. The Balmer decrement is defined by the ratio of the line intensity in frequency units $D_\nu(\mathrm{H}\alpha/\mathrm{H}\beta) \equiv I_\nu(\mathrm{H}\alpha)/I_\nu(\mathrm{H}\beta)$. The Balmer decrement, as measured from spectra, relies on line fluxes, because the line intensity is broadened by effects due to both the intrinsic properties of the emitting gas and the instrumentation used during the observation. The comparison of measured flux-ratios to

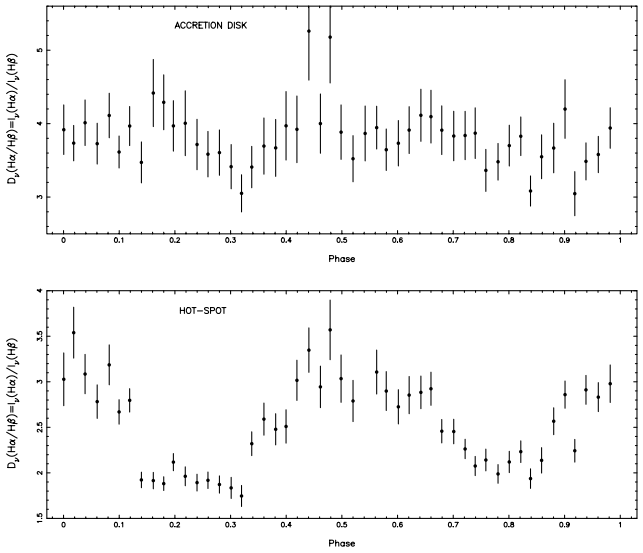

Figure 5. The Balmer decrement, $D_\nu(\mathrm{H}\alpha/\mathrm{H}\beta)$, versus orbital phase both for the accretion disc (top) and hotspot (bottom).

tabulated intensity-ratios assumes that the emission lines of interest have identical profiles, each broadened in a similar way. We observe Balmer lines which are far from being identical in shape; however, table 6 of Paper I shows that time-averaged disc profiles have *identical* velocity broadening. Deblending of the components is not possible without a complex model of hotspot shape and accretion disc structure; thus we measured the peak intensity for each component, on continuum-subtracted spectra. We measured the disc emission at each phase using only the red or blue line peak, whichever was unaffected by the hotspot emission at the given phase. The hotspot line intensity has always some underlying disc emission blending, except near phases ∼0.3 and ∼0.84, when the hotspot emission is at the centre of the emission line and the relative contribution from the accretion disc is negligible. The top panel of Fig. 5 shows that the Balmer decrement within the accretion disc is approximately constant throughout the orbit with an average value of $D_\nu(\mathrm{H}\alpha/\mathrm{H}\beta) = 3.82$, which is larger than the predicted value of $D_\nu(\mathrm{H}\alpha/\mathrm{H}\beta) \sim 1$ for an optically thick accretion disc (Williams 1980, 1983). $I_\nu(\mathrm{H}\alpha)$ and $I_\nu(\mathrm{H}\beta)$ each show phase-dependent modulations, implying a non-uniform accretion disc emission, but their ratio remains constant. However, despite the uncertainties, the Balmer decrement in the accretion disc shows a clear trend around phase 0.3 toward higher opacities. The bottom panel of Fig. 5 shows the hotspot Balmer decrement versus orbital period. The Balmer decrement here is strongly phase-dependent and shows two deep minima at phase intervals 0.2–0.3 and 0.8–0.84, i.e., when observing perpendicular to the stream trajectory at the hotspot position and measuring the hotspot line intensities without any underlying accretion disc emission. The hotspot Balmer decrement is $D_\nu(\mathrm{H}\alpha/\mathrm{H}\beta) \sim 2$. The value of $D_\nu(\mathrm{H}\alpha/\mathrm{H}\beta)$ outside phases 0.2–0.3 and 0.8–0.84 is ∼3 and approaches the average accretion disc Balmer decrement when the hotspot emission is weak. In the hotspot, $I_\nu(\mathrm{H}\beta)$ shows a stronger modulation around the orbit than $I_\nu(\mathrm{H}\alpha)$, which is largely biased by the underlying accretion disc emission.

The Balmer decrement provides information about the gas temperature and density where the emission line forms; it gives a unique gas density for each assumed temperature. However, care must be taken because different temperatures may give the same value of the Balmer decrement, depending on the assumption of

optically thick or optically thin emission lines. In the interpretation of our results we mainly use models by Williams (1991), who modelled emission lines in optically thin accretion discs. He computed Hβ strengths and Balmer decrements for a grid of temperatures, orbital inclinations, and mid-plane nucleon densities. In Fig. 6 we plot the results of Williams (1991), together with the Balmer decrement we measure at the hotspot (lower horizontal line) and the accretion disc (upper horizontal line) in WZ Sge.

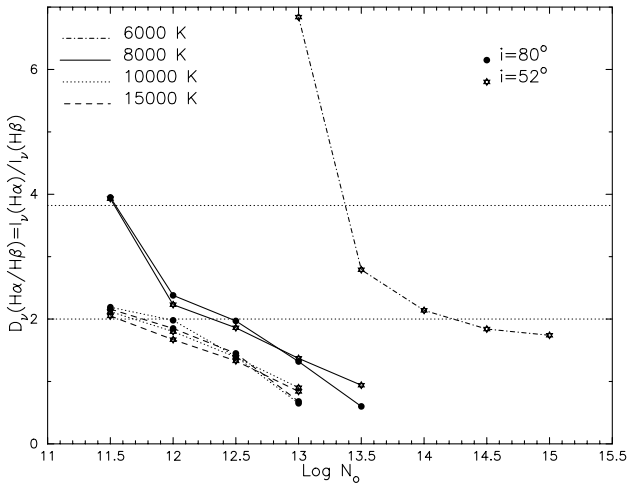

Figure 6. Balmer decrement, $D_\nu(\mathrm{H}\alpha/\mathrm{H}\beta)$, as predicted by Williams (1991) for optically thin disc emission lines. Each line represents the Balmer decrement as function of the mid-plane accretion disc density, $N_o\,\mathrm{cm}^{-3}$, for a given temperature and orbital inclination. The models for $T = 8000$, 10 000 and 15 000 K, all approach $D_\nu(\mathrm{H}\alpha/\mathrm{H}\beta) \sim 1$ at high density ($\log N_o \sim 13.0 - 13.5$), as expected for an optically thick gas. The horizontal lines mark the Balmer decrement measured for the accretion disc [$D_\nu(\mathrm{H}\alpha/\mathrm{H}\beta) = 3.82$] and the hotspot [$D_\nu(\mathrm{H}\alpha/\mathrm{H}\beta) = 2$] in WZ Sge.

Table 3. Results of fitting the radial velocity curves (see Fig. 7).

Line	Rest wavelength Å	V/R crossing ϕ_o	K_1 amplitude km s^{-1}	Systemic velocity (γ) km s^{-1}
Hβ	4861.33	0.1910 ± 0.0058	82.0 ± 2.5	-84.6 ± 2.0
Hα	6562.7725	0.1331 ± 0.0061	67.9 ± 2.8	-71.4 ± 1.9
Paβ	12 818.1	0.246 ± 0.038	46.2 ± 8.5	10.4 ± 7.0
He I	20 581.3	0.157 ± 0.014	121.4 ± 12.6	144.1 ± 9.2
Brγ	21 655.3	0.228 ± 0.023	108 ± 15	208 ± 11

The value of $D_\nu(\mathrm{H}\alpha/\mathrm{H}\beta) = 2$ for the hotspot region corresponds to a blackbody optically thick emission with a temperature of $T < 5000$ K. This decrement apparently matches a number of observed Balmer decrements in CVs (Williams 1983). However, because we observe the He I emission line at 2.06 μm, parts of the hotspot region must be at least 15 000 K (see Section 3). An optically thin gas with a temperature of 15 000 K and a Balmer decrement of 2 corresponds to a gas density of $\log N_o = 11.5$ in Williams' model (see Fig. 6), which is lower than the derived gas density within the accretion disc (see below). The gas density in the stream is expected to be 3 to 4 times larger than the gas density within the accretion disc (Lubow & Shu 1976). We thus conclude that the hotspot is at least partially optically thick and characterized by a steep temperature gradient. The Balmer emission lines form downstream from the initial impact region from a relatively low temperature ($T \sim 5000$ K) optically thick gas, and the He I 2.06-μm emission line forms in the outer stream-impact region where the temperature is higher (see Section 3).

The Balmer decrement $D_\nu(\mathrm{H}\alpha/\mathrm{H}\beta) = 3.82$ of the gas within the accretion disc would correspond to a blackbody of temperature $T \sim 3400$ K. However, we expect the temperature to be higher, as in an optically thick α-disc the temperature is never expected to fall below 6000 K over a wide range of mass accretion rate (Williams 1980). Moreover, ratioed Doppler tomograms and radial disc profile of WZ Sge (see Paper I) suggest a partially optically thin accretion disc. We conclude that the accretion disc is optically thin in the Balmer emission lines. According to Williams (1991) a Balmer decrement of $D_\nu(\mathrm{H}\alpha/\mathrm{H}\beta) = 3.82$ corresponds to an optically thin gas of temperature 6000 K and density $\log N_o \sim 13.5$ (see Fig. 6). A roughly similar value of $\log N_\mathrm{e} \simeq 13$ for gas at a temperature of $T = 5000$ K may be derived from Drake & Ulrich (1980) models. Drake & Ulrich, using the escape probability approach, determined Balmer decrements and hydrogen lines strength for an infinite slab of gas at various opacities, temperatures, and densities. We can use these estimates to determine the optically thin accretion disc mass assuming (i) a uniform gas density of $\log N_o = 13.2$, and (ii) a cylindrical accretion disc with radii as determined in Paper I (see also Table 6), and height $2H$ as already defined in Section 2.2. The result is an accretion disc mass of $\mathrm{M_d} \sim 5.7 \times 10^{-15}\,\mathrm{M}_\odot$, which is about 5 orders of magnitude smaller than the total mass accreted

Table 4. Orbital period, phase offset, and inclination for the sample of dwarf novae, see Fig. 9. References: (1) Schoembs & Hartmann (1983) & Bailey & Ward (1981); (2) Young, Schneider & Shectman (1981); (3) Marsh, Horne & Shipman (1987); (4) Stover, Robinson & Nather (1981); (5) Smak (1976); (6) Watts et al. (1986); (7) Barrera & Vogt (1989); (8) Marsh (1988); (9) this paper; (10) Szkody & Howell (1993); (11) Fiedler, Barwig & Mantel (1997). † Ritter & Kolb (1998).

Star name	DN type	Orbital period (d)	Phase offset $\Delta\phi = \phi_o - \phi_\mathrm{phot}$	i (deg)	Ref.
OY Car	SU	.06312	$.1167 \pm .0058$	$83.3 \pm 0.2^\dagger$	(1)
HT Cas	SU	.073647	$.095 \pm .009$	76.4	(2)
Z Cha	SU	.0745	$.0904 \pm .0017$	81.7	(3)
EM Cyg	ZC	.29090950	$.057 \pm .011$	$63 \pm 10^\dagger$	(4)
U Gem	UG	.17708	$.015 \pm .011$	$69.7 \pm 0.7^\dagger$	(5)
V2051 Oph	UG?	.062427887	$.132 \pm .020$	$80.5 \pm 2^\dagger$	(6)
CN Ori	UG	.163190	$.03 \pm .01$	65→70	(7)
IP Peg	UG	.15820	$.067 \pm .008$	79.3 ± 0.9	(8)
WZ Sge	SU	.05668684707	$.1620 \pm .0042$	75 ± 2	(9)
DV UMa	SU?	.0859722	$.10 \pm .02$	72	(10)
HS 1804 + 6753	UG	.2099370	$.044 \pm .002$	84.2 ± 0.6	(11)

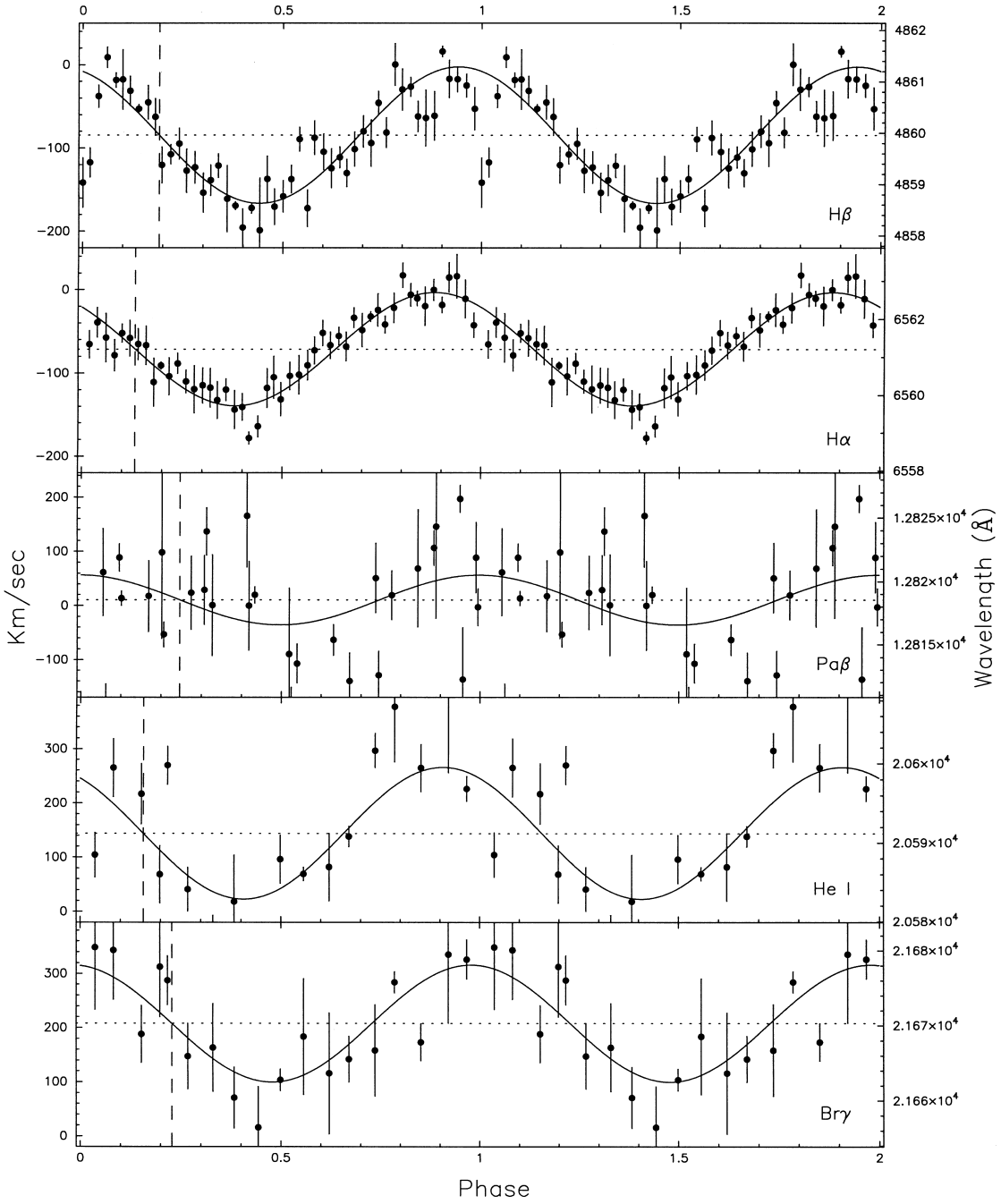

Figure 7. The radial velocity measurements and their best-fitting sine curves. Phasing is based on the photometric eclipse ephemeris of Skidmore (1998); the period was fixed at the orbital period, while the amplitude K_1 and the phase ϕ_o were free parameters in the fit. The red-to-blue crossing of each line is shown as a vertical dashed line. The mean wavelength or systemic velocity, γ, is shown as a horizontal dotted line.

during the interoutburst period ($\sim 10^{-9}\,M_\odot$; Smak 1993). It is also $\sim$4 orders of magnitude smaller than the critical mass (i.e., the maximum accretion disc mass before an outburst) expected in low mass transfer rate systems.[2] However, typical values for the mass transfer rates and critical masses have been computed using the assumption of α-disc models which are optically thick and cannot therefore be compared directly with optically thin gas models. Williams (1991) predicts an accretion disc that is only partially optically thin at a mass transfer rate of $\dot{M} \sim 10^{-11}\,M_\odot\,yr^{-1}$, the optically thin region starting from a radius of 5×10^9 cm, outward. This value seems in quite good agreement with the radius of $r \sim 2.6 \times 10^9$ cm at which we observe the transition of the Balmer line ratio from the optically thick to optically thin case (see section 4 and Fig. 7 in Paper I).

[2] We derived the value $M_{\rm crit} \sim 4 \times 10^{-11}\,M_\odot$ either using average values for the accretion disc radii and surface density as predicted by Lasota, Hameury & Huré (1995) ($R_{\rm in} \sim 4.5 \times 10^9$ cm, $R_{\rm out} \sim 1.1 \times 10^{10}$ cm, $\log \Sigma \sim 2.4$, for $\dot{M} \sim 10^{-11}\,M_\odot\,yr^{-1}$), or formula (18) in Smak (1993) with $\alpha \sim 0.003$ as predicted for TOADs by Howell, Szkody & Cannizzo (1995).

3 RADIAL VELOCITY CURVES

Optical and IR spectra were used to measure radial velocity curves for Hβ, Hα, Paβ, Brγ and He I (λ2.06-μm) emission lines. Radial velocity curve measurements were not produced for the two emission lines He I λ1.08 μm and Paγ, as they were strongly blended together.

Fig. 7 presents our radial velocity curves and their best fit for the five emission lines listed above. Each data point corresponds to the radial velocity of the emission line central wavelength. Central wavelengths were computed by using a technique similar to the Pogson's method to determine the mid-time of an eclipsing binary with an asymmetric eclipse (Glasby 1970). The radial velocity measurements were fitted by a grid-search method minimizing χ^2. The sinusoidal fitting function used was

$$v_i = \gamma + K_1 \times \sin[2\pi(\phi_i + 0.50 - \phi_o)] \quad (1)$$

where v_i is the measured velocity and ϕ_i the observed photometric phase. The fitting parameters γ, K_1, and ϕ_o are respectively the systemic velocity, the Keplerian velocity of the white dwarf around the system's centre of mass, and the red-to-blue crossing in the radial velocity curve, corresponding to secondary inferior conjunction. We added the phase shift of 0.50 in equation (1) in order to have ϕ_o exactly matching the secondary star inferior conjunction, and not the primary star inferior conjunction.

Our best-fitting parameters from each emission line represent an inconsistent set of values (see Table 3). The systemic velocity, γ, runs from negative to positive values, spanning a range $\sim$300 km s^{-1} wide. The white dwarf Keplerian velocity, K_1, runs from $\sim$46 to 120 km s^{-1}, while the red-to-blue crossing, ϕ_o, swings about phase 0.19, covering a range $\Delta\phi \simeq 0.1$ in phase. Interestingly, a similarly inconsistent set of system parameters was determined for the optical radial velocity curves of the SU UMa-type dwarf nova VY Aqr (Augusteijn 1994).

When fitting and interpreting the sinusoidal radial velocity curves, it is assumed that (i) the disc orbits with Keplerian velocity around the white dwarf, and (ii) the accretion disc follows the white dwarf motion around the binary's centre of mass. These approximations fail when hotspot emission and disc asymmetries are not negligible. Smak (1970) shows that the hotspot can induce a measured K_1 larger than the true value, and a spuriously delayed moment for inferior conjunction. Paczynski, Piotrowski & Turski (1968) explain a larger K_1 amplitude with non-Keplerian motion.

We believe that our measured radial velocity curves result from combination of two different motions: (1) the motion of the accretion disc as described at points (i) and (ii) of the previous paragraph, and (2) the motion of the gas within the hotspot region which moves along the ballistic trajectory at the stream velocity. Combination of the two velocity components in points (1) and (2) will change the amplitude and phase of a sinusoidal radial velocity curve, the largest departures occurring in systems where the hotspot emission represents the largest fraction of the total emission-line flux. An anisotropically emitting hotspot may affect the γ velocity measurements. Optically thin accretion discs are likely to be low-density gas regions (see Section 3.1), which neither affects the stream velocity of the in-falling gas, nor absorbs the flux emitted at the impact region. Thus, emission-line profiles from optically thin accretion discs are expected to be heavily biased by the hotspot emission.

The phase offset is found to be correlated with the energy required to produce each emission line. Fig. 8 shows the observed phase offset versus the excitation potential of each H emission line as given by the standard formula. Fig. 8 clearly shows a linear relationship between the observed phase offset and the emission-line energy, and implies a smeared-out hotspot region with decreasing excitation energy and temperatures as the gas moves downstream. Results similar to those in Fig. 8 may be obtained using the data in Augusteijn (1994) on VY Aqr. We fit the phase offset computed by Augusteijn for three hydrogen emission lines and found a linear relationship with almost identical slope and y-intercept as in Fig. 8.

The He I 2.06-μm emission line was not considered in Fig. 8. The He I 2.06-μm line is a transition strongly coupled with the resonant line at 584 Å. Both lines decay from the same 2^1P level, but the 584-Å transition has a probability of occurrence which is $\sim 10^3$ times larger (Najarro et al. 1994). Strong He I emission at 2.06 μm is rarely seen in astronomical objects, and is observed only in the extended atmosphere, wind and/or disc-like formations of WN and Be supergiant stars, where they form because of the high temperature, velocity and density of the out-flowing gas (15 000–30 000 K, $\sim$700 km s^{-1}, and $\sim 10^{-5}\,M_\odot\,yr^{-1}$ respectively; Najarro et al. 1994). The presence of the He I 2.06-μm emission requires the He I 584Å line to form in an optically thick, high-temperature 15 000–30 000 K region, which, in short-period dwarf novae, can only occur in the shock heated stream–disc impact region. Formation of He I 2.06 μm in a hot corona is excluded by the Doppler tomogram shown in fig. 3 of Paper I.

We interpret our results above to provide a picture for the quiescent accretion disc in WZ Sge (Fig. 4), where each hotspot emission line is likely to be aligned along the stream trajectory into the accretion disc, with the higher energy emissions arising at the higher temperature outer edge of the accretion disc impact region, and the lower energy lines primarily forming further downstream.

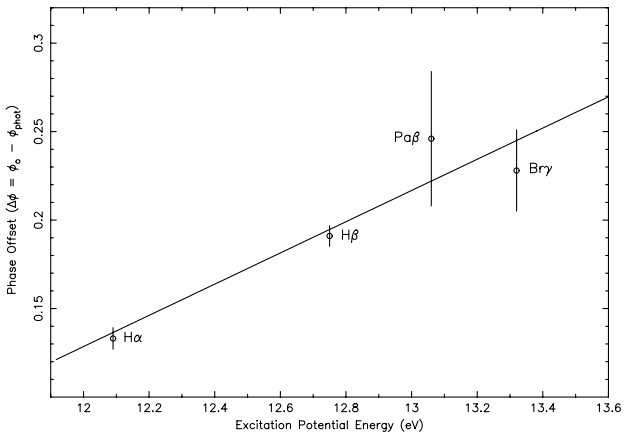

Figure 8. The linear relationship between the observed phase offset and the excitation potential of the emission line. The straight line is just to highlight the linearity of the observed distribution. The slope is 0.088 (phase/eV); the *y*-intercept is −0.93 (eV).

3.1 Phase offset as a measure of the hotspot bias

White dwarf and/or hotspot eclipses are present in the broad-band photometric light curves of many dwarf novae. In the case of the white dwarf eclipse, the observed eclipse minimum defines the time of the secondary star inferior conjunction. In systems displaying only a bright spot eclipse, the phase offset between

binary phase zero and the hotspot eclipse is small (≤0.05 in phase; Hantzios 1988), so that we still have a good idea of the time of the true binary phase zero. Similarly, when measuring radial velocity curves, we expect the spectroscopic ephemeris to match the photometric one in systems with a perfectly symmetric accretion disc, and a phase offset larger than zero in systems having asymmetries in their disc. In particular, a larger phase offset is expected in systems where the hotspot represents the main asymmetry in the accretion disc and a considerable fraction of the total emission-line flux. This is the case for WZ Sge, given that our observations average out possible short-term variation, and Doppler tomograms in Paper I show accretion disc asymmetries always considerably fainter than the hotspot emission; moreover, in Section 2 we showed the accretion disc to be optically thin. To test the hypothesis of phase offset as a measure of the hotspot bias and the optical properties of the accretion disc gas, we searched the literature for measured dwarf novae phase offsets, and we plot these values against the binary orbital period. Theory predicts low mass transfer rates in short orbital period systems (Howell, Rappaport & Politano 1997), implying low-density, possibly optically thin, accretion discs.

Phase offsets have been observed in several different CVs (Stover 1981; Watts et al. 1986; Shafter 1991), but until now there has been no explicit or systematic search for its cause. Watts et al. observed phase offsets in both nova-like and SU UMa stars, claiming that the hotspot cannot be the cause of such an offset. Stover concluded that the best candidate to explain the phase offset observed in five dwarf novae is only the hotspot. Finally, Shafter collected most of the observed phase offsets in the literature and plotted them versus the binary orbital period, but did not provide a possible explanation.

The 11 dwarf novae listed in Table 4 have been carefully selected in order to provide a homogeneous sample. This was achieved by selecting (i) high-inclination dwarf novae that show photometric eclipses, (ii) only Balmer line radial velocity curves, and (iii) publications reporting both photometric and spectroscopic analysis. Restrictions for point (i) are to avoid biases other than the hotspot, and to reduce unknown inclination effects. Point (ii) reduces the scatter in the measured phase offset by focusing on emission lines arising from regions with similar physical conditions. Finally, point (iii) guarantees consistently measured phase offset, and reduces any bias due to possible changes in the quiescent accretion state. Fig. 9 plots our selected sample which provides evidence for the expected correlation: the phase offset is larger in short orbital period systems.

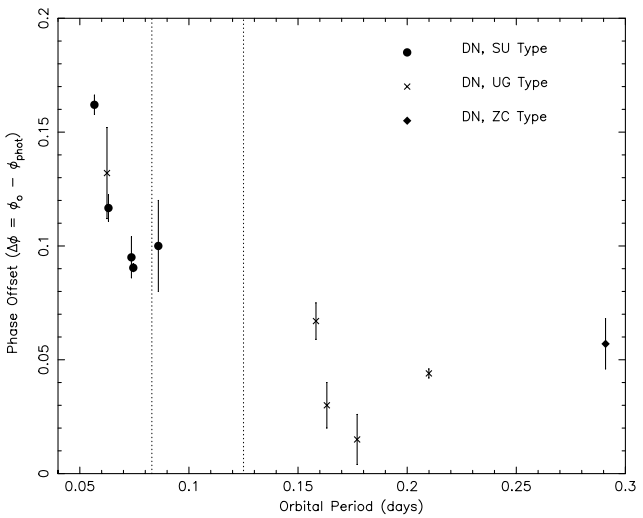

Figure 9. The observed phase offset versus orbital period. Phase offset is the delay of the spectroscopic secondary conjunction (red-to-blue crossing) as measured from the disc emission lines, with respect to the photometric eclipse minimum (i.e., the photometric phase zero). Different dwarf novae subtypes are plotted with different symbols. Dotted vertical lines delimit the period-gap.

4 ACCRETION DISC SIZE

It is possible to estimate the inner and outer accretion disc radii in a dwarf nova by measuring the emission-line wing and peak separations respectively, and assuming a Keplerian velocity. For an annulus of gas in Keplerian motion at a distance r from a white dwarf of mass $M_{\rm WD}$, orbiting at an angle i to the line of sight, the Keplerian velocity is

$$V_{\rm kep} = \sqrt{\frac{GM_{\rm WD}}{r}}\sin i. \qquad (2)$$

In a double-peaked emission line from an accretion disc, the Keplerian velocity of the outer disc radius corresponds to half the line peak separation (hereafter HPS), while the Keplerian velocity at the inner accretion disc radius corresponds to half the line wing separation (hereafter HWS).

It is important both to have reasonable system parameters and to measure HWS and HPS on unbiased spectra, i.e., spectra in which the wings and peaks of the accretion disc emission line are not affected by hotspot emission (Fig. 1, phases 0.3 and 0.84). Spectra in which the hotspot emission clearly contaminates wings and/or peaks of the accretion disc emission-line profile may provide a measure of the hotspot bias. Both HWS and HPS were measured reading the cursor position with the IRAF task *splot*. HWS values from each spectra are the average over five measurements.

4.1 Measurements on uncontaminated spectra

We selected a sample of uncontaminated phase-binned Hα and Hβ spectra. The assumption is that the hotspot emission does not affect the wings of the accretion disc emission lines. This selection criteria produced three binned Hα spectra (at phases 0.28, 0.30 and 0.32) and six binned Hβ spectra (at phases 0.28, 0.30, 0.32, 0.34, 0.82 and 0.84). We applied the same selection criteria to IR spectra, and selected two uncontaminated spectra in both the J and K bands (at phases 0.33 and ∼0.84 in each case). In case the hotspot feature was not evident (Fig. 2, J-band, phase 0.3), we select those spectra which are the closest in phase to the uncontaminated optical spectra listed above. HWS and HPS were first measured on each bin separately, and then averaged. HWS and HPS measured values are given in Table 5. We see that values from optical and IR emission lines are in good agreement each other, the exceptions being the He I 2.06-μm and Paβ lines, which apparently have smaller HPS values and larger HWS values than in the Hα, Hβ, and Brγ measurements. We applied a Student t-test (to a confidence level of $\alpha = 0.05$), to check for statistical differences between pairs of values. The test showed that the HWS values have to be considered statistically identical in all the emission lines, i.e., the same inner disc radii, while the Hβ HPS is statistically larger than the measured HPS from Hα, Brγ, He I 2.06 μm, and Paβ, thus implying a smaller outer disc radius (∼10 per cent).

Velocities from uncontaminated spectra were used in equation

(2) to compute the accretion disc radii for a variety of primary masses and inclinations (see Table 6). It is evident that small white dwarf masses ($M_{WD} < 0.5\,M_\odot$) imply a small accretion disc outer radius (<50 per cent of the primary Roche lobe radius) and a relatively large ratio R_{WD}/R_{in} (<0.5), while larger masses ($M_{WD} \geq 1\,M_\odot$) give a large outer disc radius (up to 90 per cent of the primary Roche lobe radius) and $R_{WD}/R_{in} \sim 0.07$, implying an annulus-shaped accretion disc. The input value of the white dwarf mass does not affect the ratio, $R = R_{in}/R_{out}$, which is equal to 0.2 in each case.

4.2 Measurements on the averaged spectra

Optical and IR average spectra show relatively symmetric accretion disc emission lines. This is expected because the hotspot motion, i.e., the S-wave, smoothes out the hotspot features at each phase, and evenly distributes its emission throughout the orbit. Average spectra also show broader emission lines than single spectra. This happens for two reasons: (i) the common orbital motion of the accretion disc and the white dwarf around the binary centre of mass will broaden the disc emission line by a term K_1, i.e., the white dwarf Keplerian velocity; and (ii) the wings of the hotspot emission blend with the blueshifted and redshifted accretion disc emission lines. The S-wave velocity is usually smaller than the outer disc edge Keplerian velocity (Gilliland, Kemper & Suntzeff 1986, hereafter GKS); thus we expect average spectra with broader accretion disc emission peaks and smaller peak separation than observed in single spectra. HPS and HWS from average spectra are given in Table 5. HPS values from optical and IR emission lines agree fairly well and confirm – with the exception of He I 2.06 μm and Paβ – the expectation. HWS values are also in good agreement; emission lines with larger HWS value are probably affected by high-velocity components from the hotspot. HWS and HPS measured in the averaged spectra can give information about the S-wave bias when compared with wing and peak separations from uncontaminated spectra. They also test the assumptions used in the accretion disc radii computations.

We compared HWS values from averaged and uncontaminated spectra after correction for the white dwarf orbital motion. HWS from uncontaminated spectra, and HWS from averaged spectra, K_1-subtracted, should be equal in the absence of hotspot high-velocity components. Table 7 shows that HWS values from uncontaminated spectra and K_1-subtracted averaged spectra agree very well each other in the case of Hβ and Brγ emission lines, while Hα and He I 2.06 μm have HWS values from K_1-subtracted average spectra which are ~450 and 250 km s^{-1} larger than expected in the absence of high-velocity components in the hotspot. Such components bias both radial velocity curve measures and the accretion disc radii computation. The fact that we observe the largest hotspot high-velocity component in the Hα line is consistent with Fig. 4 and the less energetic emission forming downstream in the accretion disc. High-velocity hotspot components in the Paβ emission line should be taken cautiously, because of larger uncertainties in the measurement.

It is worth noting that each average spectra was K_1-subtracted by the correspondent white dwarf orbital motion as determined in Section 3. The K_1 values from radial velocity curve fitting are biased by the hotspot and do not reflect the true orbital motion of

Table 5. Half peak separation (HPS) and half wing separation (HWS) as measured in both uncontaminated spectra and averaged spectra. Selection criteria for uncontaminated spectra are described in the text. IR measures are less certain due to low S/N data, and have not been considered in accretion disc radii computations (see text). References: (1) this paper, (2) Gilliland, Kemper & Suntzeff (1986).

Line	Uncontaminated Spectra		Average Spectra		Ref.
	HPS (km s^{-1})	HWS (km s^{-1})	HPS (km s^{-1})	HWS (km s^{-1})	
Hα	711 ± 10	1606 ± 65	676 ± 19	2133 ± 6	(1)
Hβ	762 ± 28	1692 ± 98	647 ± 15	1745 ± 23	(1)
Brγ	702 ± 66	1598 ± 50	695 ± 14	1709 ± 13	(1)
He I 2.06 μm	608 ± 66	1740 ± 97	624 ± 15	2120 ± 74	(1)
Pβ	619 ± 154	1868 ± 260	657 ± 23	2109 ± 74	(1)
Paγ			633 ± 27	–	(1)
He I 1.08 μm			646 ± 28	–	(1)
Hα			731 ± 180	~2300 ± 180	(2)

Table 6. The disc parameters determined from the line peak and line wing separations of the uncontaminated spectra. Values for q assume $M_2 = 0.058\,M_\odot$ (Smak 1993). Columns 11 and 12 are the outer disc radii normalized to the primary Roche lobe radius. References: (1) Smak (1993), (2) Spruit & Rutten (1998), (3) Cheng et al. (1997), (4) Gilliland, Kemper & Suntzeff (1986), (5) Paper I. Values from Paper I were computed applying a different method, i.e., assuming that the outer radius extends to the 3:1 tidal resonance radius and deriving M_{WD}, R_{in}, and R_{out}. The orbital inclination were taken from Smak (1993). Inner and outer radii corresponding to the HWS and HPS measured on the He I and Paβ emission lines were not computed because of their larger uncertainties and the fact that they are statistically identical to the Hα and Brγ measurements.

M_{WD} ($M_\odot$)	R_{WD} ×10^{10}cm	q M_2/M_1	i^o	R_{out} (×10^{10}cm) Hα	R_{out} Hβ	R_{out} Brγ	R_{in} (×10^{10}cm) Hα	R_{in} Hβ	R_{in} Brγ	Fraction R_{L1} Hα&$Br\gamma$	Fraction R_{L1} Hβ	Ref.
0.45 ± 0.19	0.098 ± 0.021	0.13	75	1.10 ± 0.03	0.96 ± 0.07	1.13 ± 0.21	0.22 ± 0.02	0.19 ± 0.02	0.22 ± 0.01	0.53	0.48	(1)
1.2 ± 0.25	0.039	0.05	77	2.99 ± 0.09	2.60 ± 0.19	3.07 ± 0.58	0.59 ± 0.05	0.53 ± 0.06	0.59 ± 0.04	0.93	0.84	(2)
0.3	0.055	0.19	75	0.73 ± 0.02	0.64 ± 0.05	0.75 ± 0.14	0.14 ± 0.01	0.13 ± 0.01	0.15 ± 0.01	0.43	0.38	(3)
1.1	–	0.05	80	2.78 ± 0.08	2.43 ± 0.18	2.87 ± 0.54	0.55 ± 0.04	0.49 ± 0.06	0.55 ± 0.03	0.90	0.81	(4)
0.82 ± 0.10	–	0.07	75	1.94 ± 0.06	2.04 ± 0.08	–	0.42 ± 0.26	0.26 ± 0.17	–	0.63		(5)

the white dwarf. However, because the hotspot bias is believed to increase the true K_1 value (see Section 3, Paczynski et al. 1968 and Smak 1970), the applied correction to our averaged spectra should be overestimated.

Table 5 also reports HWS and HPS as we measured by hand from the average Hα spectra in fig. 1 of GKS. Comparison of the GKS determinations with those from our averaged spectra gives us a chance to check for changes in the quiescent accretion state of WZ Sge. The data in GKS were obtained almost one year after the last outburst of WZ Sge in 1978 December and ours were obtained about 18 years after the outburst. We measured larger HWS and HPS values in the GKS spectra than in our averaged spectra. In particular, in the GKS spectra the HWS is $\sim$200 km s^{-1} larger than in our averaged spectra, while the HPS matches the values we measured on our uncontaminated spectra. Therefore we may conclude that: (i) the Hα hotspot emission high-velocity component was possibly larger one year after the superoutburst than 18 years later, (ii) the hotspot emission was probably weaker at the time of GKS observations so that it did not affect the accretion disc peak separation, and (iii) the peak separation in GKS spectra may be considered free from hotspot bias and implies constant outer accretion disc radius in the Hα emission.

Particularly interesting is the conclusion of point (iii) which claims a constant accretion disc outer radius. Indeed, the same HPS value has been observed in all quiescent spectra of WZ Sge obtained in the last 40 years (see Table 8). One possible explanation is in the assumption of the outer accretion disc radius at the 3:1 tidal resonance radius. A constant accretion disc outer radius has some important implications relating to current outburst theory. Some disc outburst theories (Meyer-Hofmeister, Meyer & Liu 1998; Truss et al. 2000) predict that, during quiescence, the outer radius slowly increases up to the 3:1 resonance radius. Once reached at the 3:1 resonance, quiescent superhumps should be present.

Table 7. Half wing separation value corrected for the white dwarf orbital motion. Each emission line measure has been corrected with the K_1 velocity determined in the corresponding radial velocity curve. † Same values as given in Table 5.

	Half Wing Separation (km s^{-1})	
Line	Uncontaminated spectra†	Averaged spectra K_1-subtracted
Hα	1606 ± 65	2065 ± 7
Hβ	1692 ± 98	1663 ± 23
Paγ	1868 ± 260	2063 ± 75
He I (2.06 μm)	1740 ± 97	1999 ± 75
Brγ	1598 ± 50	1601 ± 20

Table 8. Results of measurements of the outer disc velocity spanning 40 years. Outbursts occurred in 1946 June and 1978 December. † years since the previous outburst. References: (1) Greenstein (1957), (2) Krzeminski & Kraft (1964), (3) Gilliland, Kemper & Suntzeff (1986), (4) Smak (1993), (5) Neustroev (1998), (6) this paper.

Line	Date	Δyr†	v_{outer} (km/sec)	Ref.
Hβ	1956 Aug 15	10	720	(1)
Hγ	1956 Aug 15	10	710	(1)
Hβ	1962 Aug 4	16	720 ± 14	(2)
Hγ	1962 Aug 4	16	720 ± 14	(2)
Hα	1979 July 16	1	731	(3)
Hβ	1983 Nov 24–28	5	730 ± 30	(4)
Hγ	1983 Nov 24–28	5	730 ± 30	(4)
Hα	1994 May 30	16	747 ± 40	(5)
Hα	1996 July 27/28	18	711 ± 10	(6)
Hβ	1996 July 27/28	18	762 ± 28	(6)

4.3 Smak's method of determining R_{in}/R_{out}

The accretion disc radii ratio, $R = R_{in}/R_{out}$, is often the only value provided by authors because of the large uncertainties affecting the determination of the orbital inclination and the binary star masses. A commonly applied method to compute R is the one developed by Smak (1981).

Smak's method assumes axially symmetric accretion disc in Keplerian motion and a power-law flux distribution ($f \sim r^{-\alpha}$) for the disc emission. The R and α values depend on the parameters U, A_{84} and A_{41}, which are defined as follow: $U = res/\Delta\lambda$, with res = instrumental resolution, $A_{84} \equiv \log W_{0.8} - \log W_{0.4}$, and $A_{41} \equiv \log W_{0.4} - \log W_{0.1}$, where $W_{0.8}$, $W_{0.4}$ and $W_{0.1}$ are the emission-line widths at the fractions 0.8, 0.4 and 0.1 of the peak height above the continuum respectively.

Mennickent & Arenas (1998) applied Smak's method to WZ Sge and determined $A_{84} = 0.07$, $A_{41} = 0.1$, and $R = 0.3$ (see Table 9). A ratio $R = 0.3$ is 50 per cent larger than the value 0.2 we determined in Section 4.1. We investigated such a difference to understand whether it reflects changes in the quiescent accretion disc size or it implies inconsistencies between the Smak's method and the method described in Section 4.1. We applied Smak's method to our Hα and Hβ uncontaminated spectra and found A_{84} and A_{41} values matching those by Mennickent & Arenas (see Table 9). However, we expect a ratio $0.2 \leq R < 0.3$. Then we may conclude that: (i) the two methods are consistent and, in particular, the assumptions of axisymmetric disc and power-law flux distribution required by the Smak's method are not fundamental to the determination of R, and Smak's method may be applied also to asymmetric accretion discs such as WZ Sge; (ii) the two accretion disc radii ratio, $R = 0.3$ by Mennickent &

Table 9. Our measurements of the disc parameters from the uncontaminated spectra using the method described in Smak (1981) compared to the measurements of Mennickent & Arenas (1998). Measurements made assuming a Keplerian disc †, and the data of Neustroev (1998). References: (1) (Mennickent & Arenas 1998), (2) this paper, (3) (Neustroev 1998).

Line	A_{84}	A_{41}	U	α	R	Ref.
Hα	0.07 ± 0.02	0.104 ± 0.001	0.12	0.5	0.30	(1)
Hα	0.072	0.113	0.013	>1	>0.2	(2)
Hβ	0.077	0.122	0.016	>0.75	>0.23	(2)
Hα					0.20	(2)†
Hβ					0.20	(2)†
Hα				1.66 ± 0.19	0.08 ± 0.04	(3)

Arenas and $R = 0.2$ by us, may correspond to a real change in WZ Sge's quiescent accretion state and indicate an inward motion of the inner accretion disc radius toward the white dwarf surface (in Section 4.2 we showed that the outer disc radius remains constant during quiescence).

5 SUMMARY AND CONCLUSIONS

We observed both hotspot and accretion disc line emission to vary in shape and strength throughout an orbital period, and conclude that both the hotspot and the accretion disc are asymmetric and anisotropically emitting. We determined the gas at the impact region to have just the stream velocity, and the accretion disc is a low-density gas with little drag effects on the in-falling material from the secondary star. There are different Balmer decrements at the impact region and in the rest of the accretion disc, and we conclude that the gas has a different opacity, τ, within the two regions. In particular, the hotspot is optically thick in the lines, while the accretion disc appears to be optically thin in the lines.

Our measured radial velocity curves, from five emission lines in the optical and in the infrared are found to present an inconsistent set of system parameters. We explain this result as a bias due to the hotspot emission. In particular, we showed that the hotspot emission delays the apparent time of the secondary inferior conjunction with respect to photometric phase zero. We also show that the phase offset depends both on the excitation potential energy of the considered emission line and on the optical depth of the gas in the accretion disc. Our extended analysis of a selected sample of dwarf novae shows increasing phase offset with shorter orbital period, consistent with the idea of optically thin accretion discs in low mass transfer rate systems.

Summarizing our results from the emission-line profile analysis and radial velocity curve computations presented here, we can formulate a probable structure for the WZ Sge accretion disc. The accretion disc is generally a low-density, optically thin gas. The accretion disc is neither symmetric, nor has it a uniform gas density or temperature structure (see also Paper I). The hotspot is optically thick in the emission lines, not symmetric in shape, and not an isotropic emitter. The hotspot emission arises from a multicomponent extended region in which each emission component is not visible at all phases, and the hotspot emission varies in strength throughout the orbital period. These variable hotspot emissions lead to an extended hotspot region which does not emit strongly when viewed from the downstream direction (phase 0.5 and following), and shows a temperature gradient along the stream trajectory. Fig. 4 summarizes our conclusion.

The qualitative picture of WZ Sge provided by our observations and data analysis shows a peculiar quiescent accretion disc dissimilar to others observed at present. WZ Sge is the first short orbital period dwarf nova showing evidence of optically thin emission both in the continuum (Ciardi et al. 1998; Skidmore 1998) and in the lines. Multicolour photometry of OY Car, Z Cha and HT Cas (Marsh 1987; Wood 1990; Wood, Horne & Vennes 1992) shows evidence of quiescent accretion disc optically thin in the continuum but thick in the emission lines. This work establishes a first step toward an understanding of the spatial flux and material distribution within the WZ Sge accretion disc and other TOAD (Tremendous Outburst Amplitude Dwarf novae; Howell, Rappaport & Politano 1997) candidates.

The accretion disc radii determined in Section 4.1 show that determination of the inner and outer radii depends strongly on the assumed white dwarf mass and the binary orbital inclination. Unfortunately, white dwarf mass and radius determinations are still affected by large uncertainties. The uncertainties on the WZ Sge white dwarf parameters prevent us from uniquely determining the actual size of the accretion disc, the fraction of the primary Roche lobe it fills, or its exact shape. Whether the accretion disc extends down to the white dwarf surface or is a ring-like accretion disc as suggested by some previous studies (Mennickent & Arenas 1998; Meyer-Hofmeister et al. 1998; Howell et al. 1999) cannot be uniquely determined. We determined the accretion disc radii ratio in WZ Sge, $R = R_{\rm in}/R_{\rm out}$, to be 0.2, and observed that the outer accretion disc radius does not vary during the quiescence period. One explanation for the constant accretion disc outer radius is the assumption that the accretion disc extends to the 3:1 tidal resonance radius. One possible test of this idea would be to search for and find quiescent superhumps.

ACKNOWLEDGMENTS

The optical data used in this study were obtained by Henke Spruit and Rene Rutten with the William Herschel Telescope of the ING at La Palma. The William Herschel Telescope is operated on the island of La Palma by the Isaac Newton Group in the Spanish Observatorio del Roque de los Muchachos of the Instituto the Astrophysica de Canarias. The United Kingdom Infrared Telescope is operated by the Joint Astronomy Centre on behalf of the UK Particle Physics and Astronomy Research Council. SBH acknowledges partial support of this research from the NSF grant AST 98-19770 and from the University of Wyoming office of research. We thank Dr Peter Tamblyn for his help and information concerning He I emission.

REFERENCES

Augusteijn T., 1994, A&A, 292, 481
Bailey M. E., Ward M., 1981, MNRAS, 196, 425
Barrera L. H., Vogt N., 1989, A&A, 220, 99
Cheng F. H., Sion E. M., Szkody P., Huang M., 1997, ApJ, 484, 149
Ciardi D. R., Howell S. B., Haushchildt P. H., Allard F., 1998, ApJ, 504, 450
Drake S. A., Ulrich R. K., 1980, ApJS, 42, 351
Fiedler H., Barwig H., Mantel K. H., 1997, A&A, 327, 173
Gilliland R., Kemper E., Suntzeff N., 1986, ApJ, 301, 252 (GKS)
Glasby I. S., 1970, The Dwarf Novae. American Elesvier Publishing Company Inc., New York
Greenstein J., 1957, ApJ, 126, 23
Hantzios P. A., 1988, PhD thesis, Ohio State Univ.
Horne K., Marsh T. R., 1986, MNRAS, 218, 761
Howell S. B., Szkody P., Cannizzo J. K., 1995, ApJ, 439, 337
Howell S. B., Rappaport S., Politano M., 1997, MNRAS, 287, 929
Howell S. B., Ciardi D. R., Szkody P., Van Paradijs J., Kuulkers E., Cash J., Sirk M., Long K., 1999, PASP, 111, 342
Krzeminski W., Kraft R., 1964, ApJ, 140, 921
Lasota J. P., Hameury J. M., Huré J. M., 1995, ApJS, 53, 523
Lubow S. H., Shu F. H., 1976, ApJ, 207, L53
Marsh T., 1987, MNRAS, 228, 779
Marsh T., 1988, MNRAS, 231, 1117
Marsh T. R., Horne K., Shipman H. L., 1987, MNRAS, 225, 551
Mennickent R., Arenas J., 1998, PASJ, 50, 333
Meyer-Hofmeister E., Meyer F., Liu B., 1998, A&A, 339, 507
Najarro F., Hillier D. J., Kudritzki R. P., Krabbe A., Genzel R., Lutz D., Drapatz S., Geballe T. R., 1994, A&A, 285, 573
Neustroev V., 1998, Astron. Rep., 42, 748
Paczynski B., Piotrowski S. L., Turski W., 1968, ASS, 2, 254

Patterson J., Augustejin T., Harvey D. A., Skillman D. R., Abbott T. M. C., Thotstensen J., 1996, PASP, 108, 748
Ritter H., Kolb U., 1998, A&AS, 129, 83
Schoembs R., Hartmann K., 1983, A&A, 128, 37
Shafter A. W., 1991, Fundamental Properties of Cataclysmic Variable Stars, Proceeding of the 12th North American Workshops on Cataclysmic Variables, p. 39
Skidmore W., 1998, PhD thesis, Univ. Keele
Skidmore W., Mason E., Howell S. B., Ciardi D. R., Littlefair S., Dhillon V. S., 2000, MNRAS, 318, 429 (Paper I, this issue)
Smak J., 1970, Acta Astron., 20, 311
Smak J., 1976, Acta Astron., 26, 277
Smak J., 1981, Acta Astron., 31, 395
Smak J., 1993, Acta Astron., 43, 212
Spruit H., Rutten R., 1998, MNRAS, 299, 768
Stover R. J., 1981, ApJ, 249, 673
Stover R. J., Robinson E. L., Nather R. E., 1981, ApJ, 248, 696
Szkody P., Howell S. B., 1993, ApJ, 403, 743
Truss M., Murray J., Wynn G., Edgar R., 2000, MNRAS, in press
Warner B., 1995, Cataclysmic Variable Star. Cambridge Univ. Press, Cambridge, p. 691
Watts D., Bailey J., Hill P., Greenhill J., McCowage C., Carty T., 1986, A&A, 154, 197
Williams R. E., 1980, ApJ, 235, 939
Williams G. A., 1983, ApJS, 53, 523
Williams G. A., 1991, AJ, 101, 1929
Williams G. A., Shipman H. L., 1988, ApJ, 326, 738
Wood J. H., 1990, MNRAS, 243, 219
Wood J. H., Horne K., Vennes S., 1992, ApJ, 385, 294
Young P., Schneider D. P., Shectman S. A., 1981, ApJ, 245, 1043

This paper has been typeset from a TEX/LATEX file prepared by the author.